GeoStorage

Vol. 2, No. 3, p. 258-273, 2026

Research article

Dynamic Reconstruction of Working-Gas Space in High-Water-Cut Oil Reservoirs Converted to Underground Gas Storage

Qian Zhang[1,2], Dewen Zheng[1,2], Lei Shi[1,2*], Qiqi Wanyan[1,2], Chun Li[1,2], Hongcheng Xu[1,2], Jieming Wang[1,2]

[1] *PetroChina Research Institute of Petroleum Exploration & Development, Beijing 100083, China*
[2] *CNPC Key Laboratory of Oil and Gas Underground Storage Engineering, Langfang, Hebei 065007, China*

Keywords:
Underground gas storage
high-water-cut oil reservoir
cyclic injection-withdrawal
three-phase relative permeability
hysteresis
working-gas capacity

Cited as:
Zhang Q, Zheng DW, Shi L, et al. 2026. Dynamic Reconstruction of Working-Gas Space in High-Water-Cut Oil Reservoirs Converted to Underground Gas Storage. *GeoStorage*, 2(3), 258-273.
https://doi.org/10.46690/gs.2026.03.05

Abstract:
Conversion of mature waterflooded oil reservoirs to underground gas storage (UGS) is controlled by cyclic gas-oil-water flow rather than by simple repressurization of a depleted hydrocarbon pore volume. At the onset of storage operation, residual oil and movable or capillary-trapped water occupy a substantial fraction of the pore space, whereas the connected gas volume required for repeatable injection-withdrawal cycling is only partially developed. This review synthesizes the conversion process from pore to reservoir scale around four coupled controls: liberation of liquid-occupied pore volume, establishment and persistence of gas-phase connectivity, hysteretic relative-permeability and capillary-pressure responses to drainage-imbibition reversals, and the resulting injectivity, withdrawal deliverability, and working-gas capacity. Evidence from cyclic core flooding, high-pressure/high-temperature (HPHT) micromodel experiments, special core analysis (SCAL), reservoir simulation, and field studies indicates that usable gas-storage space is a dynamic, history-dependent flow property rather than a fixed fraction of geological pore volume. A phenomenological three-stage evolution is identified, comprising initial flow-path establishment, sweep expansion, and quasi-stable cycling, with channel-dominated and balanced-expansion responses representing two mechanistic end members. The review further links pore-scale trapping, film flow, remobilization, gas-oil compositional mass transfer, reservoir heterogeneity, and aquifer influx to cycle-conditioned saturation functions and reservoir-scale performance. Liquid-displacement metrics are therefore most informative when evaluated jointly with gas saturation, gas mobility, sweep efficiency, and cyclic recoverability. This distinction prevents produced-liquid volume from being conflated with field-scale working-gas volume. The central implication is that liquid drainage and gas-phase connectivity must evolve concurrently before geometrical pore volume can be converted into repeatedly recoverable working-gas space.

1 Introduction

Underground gas storage (UGS) provides seasonal supply balancing and peak-shaving deliverability at rates relevant to regional gas-system security. The 2025 International Gas Union (IGU) survey reports 699 operating UGS facilities worldwide as of April 2025, with 424 billion cubic metres (bcm) of working-gas volume (WGV) and approximately 7,371 million m^3/d of potential withdrawal capacity. Depleted gas fields account for 314 bcm (74%) of global WGV, aquifers 47 bcm (11%), salt caverns 40 bcm (9%), and oil fields 23 bcm (6%) (IGU Storage Committee, 2025). Oil-field WGV is concentrated in North America (18.386 bcm), the Commonwealth of Independent States (CIS; 3.500 bcm), Europe (1.264 bcm), and Asia (0.215 bcm) (IGU Storage Committee, 2025). Because global project counts are not consistently disaggregated for oil-reservoir conversions, this review reports the verified WGV distribution rather than inferring a facility count (Fig. 1). The global oil-field WGV is reported as 23 bcm after rounding, whereas the regional values sum to 23.365 bcm. The IGU dataset compiles

Yandy Scientific Press

* Corresponding author.
E-mail address: qzhang@mail.whrsm.ac.cn (Zhang Q); zdw698@petrochina.com.cn (Zheng DW); easonlyr@163.com (Shi L); wanyanqq@petrochina.com.cn (Wanyan QQ); lichun30@petrochina.com.cn (Li C); xuhongc@petrochina.com.cn (Xu HC); jieming@petrochina.com.cn (Wang JM)

Received Aug. 10, 2026; revised Aug. 15, 2026; accepted Sep. 1, 2026; available online Sep. 9, 2026.

information collected during 2023-2025, with operating-facility status reported as of April 2025.

China illustrates the growing interest in this branch of UGS development. The IGU survey lists 25 Chinese UGS facilities, 19.83 bcm of WGV, and 220 million m^3/d of potential withdrawal capacity, with WGV increasing by 6 bcm relative to the 2022 survey (IGU Storage Committee, 2025). Effective peak-shaving working gas in 2024 was reported as 6.2% of annual gas consumption, below the 10% storage-capability target (Zheng et al., 2025). Consequently, current research on oil-reservoir conversion emphasizes secondary gas-cap development and control, coupled gas-storage/gas-drive operation, gas-liquid displacement, interphase mass transfer, and performance-index design (Yu et al., 2026).

Documented field experience includes both long-lived international precedents and recent Chinese conversions (Tab. 1). Aliso Canyon was converted from an oil field to gas storage in the early 1970s, whereas Reitbrook operated as UGS from 1973 to 2014 while oil production continued (California Geologic Energy Management Division , CalGEM; Bontemps et al., 2011; Perreaux et al., 2015). In China, Jing 58 represents a depleted gas-cap oil reservoir, Shuang 6 a faulted gas-cap oil field, and Nanpu-1 a faulted depleted oil reservoir that entered formal offshore operation in November 2024 (Jiang et al., 2021; Ding et al., 2015; Song et al., 2025; Gao et al., 2025; China News Service, 2024). These cases show that oil-reservoir UGS spans markedly different gas-cap histories, fault architectures, water invasion, and residual-liquid states.

Depleted gas reservoirs are commonly preferred for porous-media UGS because prior depletion partially constrains pressure history, deliverability, and containment performance. Waterflooded oil reservoirs are fundamentally different: they inherit a waterflood-conditioned oil-water saturation field containing residual oil, movable water, wetting films, and local liquid banks. Injected storage gas must invade this liquid-rich pore network, establish a percolating gas phase, and preserve sufficient connectivity through withdrawal and reinjection. By contrast, repressurization of a depleted gas reservoir predominantly alters gas PVT behavior, reservoir pressure, gas-water contact position, and aquifer response. Geological pore volume therefore represents only an upper bound on the pore volume that can participate effectively in converted oil-reservoir UGS.

Field and laboratory studies resolve different parts of this conversion. Fracture-matrix exchange, well placement, and fluid properties affect field performance (De Kok et al., 2008; Bontemps et al., 2011; Eren and Polat, 2020). Cyclic oil-reservoir experiments show continuing changes in multiphase-flow response, liquid production, and gas-accessible pore volume after breakthrough (Zhang et al., 2022; Tang et al., 2025; Zhang et al., 2026a,c). Pore-scale imaging identifies films, ganglion trapping, Haines jumps, snap-off, and connectivity changes, including direct HPHT observations in hydrocarbon-gas-oil-water systems (Zhang et al., 2026b).

Relative permeability and capillary pressure provide the constitutive closure that links pore-scale phase configuration to multiphase Darcy flow. Cyclic models commonly combine drainage and imbibition bounding curves with hysteresis scanning rules, whereas classical formulations generally retain fixed bounding curves after calibration (Land, 1968; Killough, 1976; Carlson, 1981; Honarpour et al., 1986). This assumption is most uncertain during early conversion, when liquid phases are actively remobilized and gas-phase connectivity is being reconstructed. Storage experiments and simulations confirm the importance of hysteresis (Wang et al., 2022, 2026), but available data do not yet demonstrate whether three-phase bounding functions evolve systematically from cycle to cycle (Larsen and Skauge, 1998; Shahverdi and Sohrabi, 2015; Gao et al., 2023).

Recent GeoStorage articles have reviewed geological storage engineering (Liu et al., 2025), structural capacity controls (He et al., 2026), fluid migration in depleted oil and gas reservoirs (Jiang et al., 2026), and cyclic gas-water relative permeability (Wang et al., 2026). The narrower question addressed here is how liquid-occupied pore volume in a waterflooded, high-water-cut oil reservoir becomes gas-accessible, hydraulically connected, and repeatedly recoverable while gas, oil, and water continue to interact. The governing problem is therefore progressive reconstruction of usable storage space under cyclic three-phase flow, rather than simple gas migration through a depleted reservoir.

This review follows that reconstruction across scales. Natural-gas storage in converted oil reservoirs is the primary focus; CO2 storage, underground hydrogen storage, WAG, and related studies are invoked only where their underlying multiphase-flow mechanisms are transferable. Pore-scale imaging resolves displacement mechanisms, special core analysis (SCAL) constrains saturation functions, long-core experiments reveal liquid mobilization and flow-path competition, and reservoir/field studies establish engineering relevance. Here, gas-accessible pore volume denotes pore volume contacted by injected gas. Working-gas space denotes the hydraulically connected fraction that can repeatedly participate within the operating pressure window; it is distinct from field WGV, which is the surface-standard gas inventory cycled between prescribed lower and upper operating pressures. Dynamic convertibility denotes the capacity of an inherited liquid-rich reservoir state to develop such recoverable gas-storage space.

2 High-water-cut oil reservoirs as a distinct UGS conversion system

2.1 High-water-cut oil reservoirs as a distinct UGS conversion system

The initial condition of a candidate reservoir is controlled by its depletion and waterflood history. Depletion modifies pressure and phase behavior, whereas waterflooding preferentially advances through high-mobility pathways and leaves residual or bypassed oil in smaller pores, dead-end elements, corners, and wetting films. Prior to storage-gas injection, the reservoir therefore contains a heterogeneous, history-conditioned oil-water saturation field rather than a uniformly depleted pore volume. Similar field-scale water cuts can mask major differences in sweep efficiency, residual-oil topology, capillary entry pressure, and subsequent gas accessibility because depositional architecture, permeability contrast, wettability, and waterflood history differ.

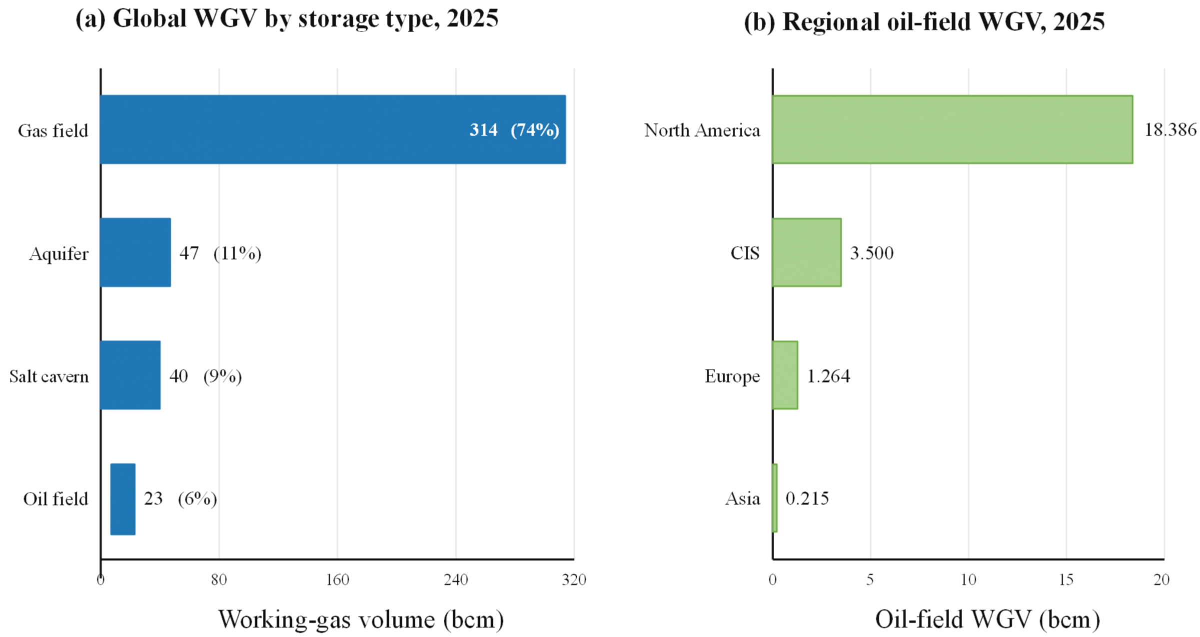

Fig. 1 Global context of oil-field underground gas storage in 2025. (a) Global working-gas volume (WGV) by storage type; (b) regional distribution of oil-field WGV

Tab. 1 Representative documented oil-reservoir UGS precedents and verified construction/operation status

Facility (country)	Oil-reservoir setting	Verified construction / operation status	Reported storage metric	Relevance to this review
Aliso Canyon (USA)	Former oil field; oil production began in 1939	Converted to natural-gas storage in the early 1970s; limited operation resumed after the 2017 safety review	Largest natural-gas storage facility in California	Long-duration conversion highlights well-integrity, surveillance, and regulatory constraints (California Geologic Energy Management Division , CalGEM).
Reitbrook (Germany)	Mature complex oil field	Oil production 1937-1963; gas blowdown 1963-1973; UGS 1973-2014; oil production continued during storage	Historical UGS lifecycle; additional oil was produced during storage	Field precedent for coupled storage and residual-oil mobilization (Bontemps et al., 2011; Perreaux et al., 2015).
Jing 58 (China)	Depleted sandstone oil reservoir with a gas cap	Oilfield development ended in 2006; subsequently reconstructed as UGS	Design capacity 0.81 bcm; WGV 0.39 bcm	Chinese precedent for gas-cap oil-reservoir conversion and staged pressure/volume design (Jiang et al., 2021).
Shuang 6 (China)	Shuangtaizi oil field; gas cap, multilayer sandstone, well-developed faults	Developed as UGS in 2014; later field studies continue to address cyclic-operation and fault-stability control	Reported WGV 1.60 bcm in the 2015 national survey	Demonstrates the coupling of multiphase conversion with faulted-reservoir integrity (Ding et al., 2015; Song et al., 2025).
Nanpu-1 (China)	Faulted depleted oil reservoir; offshore Bohai Bay setting	Pilot testing began in 2021; formal operation started 26 Nov 2024 as China's first offshore UGS	Design effective capacity 1.814 bcm; WGV 1.052 bcm	Extends oil-reservoir conversion to offshore fault-block settings, where pressure limits and sealing integrity are critical (Gao et al., 2025; China News Service, 2024).

This inherited fluid distribution limits immediately available pore volume and controls gas-entry thresholds, phase mobility, and connectivity after flow reversal. Waterflooding also leaves hydraulic memory in the saturation field. The first storage-gas injection therefore starts from oil-water interfaces and gradients created by depletion and water injection rather than from idealized primary drainage. Early operation is a transition in which a waterflooded oil reservoir is reorganized into a gas-bearing cyclic storage system.

Residual-oil configuration is governed by wettability and pore geometry; consequently, gas invasion may remobilize some oil clusters while bypassing others (Gao et al., 2022; Yang et al., 2021). Pore-throat heterogeneity determines the distribution of capillary entry pressures and the selection of preferential flow paths (Xie et al., 2017). At reservoir scale, buoyancy and stratigraphic heterogeneity amplify these pore-scale preferences: gas preferentially migrates toward structural highs and higher-mobility intervals, whereas water tends to reoccupy lower or finer-grained zones during pressure decline. Candidate reservoirs should therefore be screened as history-dependent multiphase-flow systems rather than solely by static pore volume and absolute permeability.

2.2 Comparison with depleted gas-reservoir storage

Tab. 2 summarizes the main differences from depleted gas-reservoir UGS. Depleted gas reservoirs still require treatment of aquifer influx, gas-water relative permeability, near-well liquid accumulation, cushion gas, and gas-water transition-zone movement. Cyclic operation can reorganize these gas-water systems (Shi et al., 2012, 2013; Zheng et al., 2026; Lysyy et al., 2021, 2022; Kanaani et al., 2022). Oil-reservoir conversion adds gas-oil mass transfer, swelling and viscosity change, oil-film connectivity, and genuinely three-phase relative-permeability and capillary-pressure behavior.

Neither absolute permeability nor geological pore volume alone is sufficient for conversion screening. High permeability may provide high initial injectivity and rapid pressure communication, but it can also accelerate gas breakthrough and preferential channeling. Moderately permeable rock may establish gas-phase connectivity more slowly while continuing to recruit secondary pathways over repeated injection-withdrawal reversals. Aquifer support can sustain pressure yet return water during withdrawal, and residual oil both occupies potential gas-storage pore volume and remains susceptible to remobilization by hydrocarbon gas. The net conversion response therefore depends on the coupled rock-fluid state and the imposed pressure-rate trajectory.

2.3 The storage objective differs from gas EOR

Gas-enhanced oil recovery (EOR) literature provides useful mechanistic insight into gas-oil displacement, miscibility, gravity segregation, and mobility control (Jerauld, 1998; Ding et al., 2017; Gbadamosi et al., 2018; Anikin et al., 2025), but the engineering objective of UGS is fundamentally different. UGS performance is assessed by repeatable working-gas capacity, injectivity, withdrawal deliverability, produced-gas quality, allowable operating-pressure window, cushion-gas requirement, containment, and well integrity. Incremental oil recovery may be an advantageous co-benefit during conversion, but it does not demonstrate establishment of a repeatable working-gas inventory.

Liquid drainage from gas-contacted rock releases pore volume, but that volume contributes to working-gas capacity only if the gas phase can access it, remain hydraulically connected, and be withdrawn within the operating pressure window. A dominant channel may yield substantial local liquid production while leaving a large fraction of the reservoir unswept; conversely, gradual recruitment of secondary pathways over several cycles may add recoverable gas volume. The relevant conversion sequence is therefore liquid mobilization, gas occupancy, gas-phase connectivity, and cyclic recoverability (Tab. 3).

3 Progressive development of gas-accessible pore volume and working-gas space

3.1 Gas-accessible space develops over repeated cycles

Cyclic experiments indicate that operationally effective gas-accessible pore volume is not established by a single gas flood. Tests that reproduce depletion, waterflooding, initial gas injection, withdrawal, and repeated cycling show continued evolution of gas saturation, liquid production, and gas mobility after first gas breakthrough (Zhang et al., 2022; Tang et al., 2025; Zhang et al., 2026a,c). A critical distinction must therefore be maintained among total geological pore volume, gas-contacted pore volume, and the smaller connected gas volume that can repeatedly participate in cyclic storage.

During initial gas injection, the nonwetting gas phase preferentially invades larger or better-connected pore throats once local capillary entry pressure is exceeded. A spanning gas pathway may form before adjacent oil- and water-filled pores are substantially mobilized. Following breakthrough, gas flow can remain focused within this low-resistance pathway. Withdrawal imposes an imbibition-dominated reversal: wetting phases reenter the pore network, gas clusters may disconnect by snap-off, and local oil-water banks redistribute. Reinjection therefore starts from an altered saturation topology and hysteresis scanning state rather than retracing the preceding drainage path.

Repeated injection-withdrawal reversals can remobilize liquids outside the earliest gas pathway and progressively enlarge the gas-accessible region. Experiments on converted oil-reservoir systems report increasing liquid displacement and gas-accessible pore volume across successive operating stages, although the magnitude depends on pore structure, wettability, fluid properties, gas composition, operating-pressure window, and cycling protocol (Zhang et al., 2026a,c). Because later experimental stages may also employ wider pressure windows, observed improvement should be attributed to the combined effects of flow reversal, saturation-history perturbation, and pressure-window evolution rather than to cycle number alone.

3.2 Three stages of storage-space reconstruction

A phenomenological three-stage description is useful for organizing the available evidence. During pathway establishment, injected gas first occupies the most conductive connected routes near injection intervals and structural highs. Gas saturation and apparent mobility can increase rapidly, yet the participating gas volume remains limited because much of the reservoir is still liquid rich. For a prescribed injection rate, pressure buildup or near-well pressure gradient can therefore remain high while gas communication is confined to a relatively small connected volume.

During sweep expansion, continued cycling and liquid production extend gas access beyond the initial preferential path-

Tab. 2 Fundamental differences between depleted gas-reservoir UGS and high-water-cut oil-reservoir conversion

Attribute	Depleted gas-reservoir UGS	High-water-cut oil-reservoir conversion
Dominant inherited fluids	Gas + formation water	Residual oil + injected/formation water + locally retained gas
Initial gas-connected pore space	Usually extensive	Limited or discontinuous in many zones
Primary conversion task	Repressurization and working/cushion gas definition	Progressive release and connection of gas-accessible pore space
Main multiphase flow	Gas-water	Gas-oil-water, with possible gas-oil mass transfer
Key history effect	Water invasion and gas trapping	Waterflood history + residual-oil architecture + cyclic trapping
Important constitutive functions	Gas-water relative permeability and capillary pressure	Three-phase relative permeability/capillary pressure and hysteresis/scanning behavior
Main early-cycle constraint	Pressure support and water encroachment	Gas-entry threshold, liquid mobilization, and pathway establishment
Main capacity uncertainty	Pressure-volume relation and aquifer response	Participating pore volume, gas sweep/connectivity, and liquid return

ways. Residual oil and movable water are redistributed, additional rock volume is contacted, and areal and vertical gas sweep increase. Recoverable gas-accessible pore volume may grow most rapidly during this stage, provided that new gas pathways remain connected during withdrawal. Pressure response also becomes less dominated by the immediate near-well region as a larger connected storage volume participates in the cycle.

The third stage is quasi-stable cycling. Main gas pathways persist, incremental liquid production declines, and further changes in contacted volume become localized. Quasi-stable does not imply complete conversion: low-permeability layers, capillary end zones, isolated compartments, and aquifer-supported intervals may remain outside the working-gas system. Operating priorities therefore shift from establishing connectivity, to expanding sweep, to maximizing repeatable withdrawal and deliverability within integrity limits (Fig. 2).

3.3 Channel-dominated and balanced-expansion end members

Reservoirs need not progress through these stages in the same manner. Comparative long-core data from sandstone systems with contrasting rock-fluid properties support two useful mechanistic end members for describing storage-space development (Zhang et al., 2026c). In a channel-dominated response, gas establishes high-conductivity pathways early, producing rapid gains in injectivity and apparent gas mobility. The same behavior can subsequently become limiting: once a small number of preferential paths carry most of the flow, additional cycling may recruit little pore volume outside those paths. A reservoir judged only by early pressure drop or injection rate can therefore appear more favorable than indicated by its recoverable working-gas space.

A balanced-expansion response develops more gradually. In the available long-core datasets, delayed gas connectivity is associated with stronger capillary-entry constraints and continued recruitment of secondary pathways during repeated pressure reversals, allowing liquid mobilization and gas-accessible volume to expand over a broader fraction of the pore network. These observations should not be interpreted as a simple permeability rule. Permeability, pore-throat geometry, fluid viscosity, wettability, and heterogeneity covary in the available experiments, preventing their individual effects from being isolated. The classification is therefore most appropriately used to distinguish contrasting modes of storage-space evolution: rapid flow concentration within a few conductive pathways versus slower expansion of a broader connected gas region.

This distinction also demonstrates why injectivity should not be optimized independently of storage-space development. A high instantaneous injection rate may reinforce an established preferential channel without increasing areal or vertical sweep, whereas a controlled pressure-rate trajectory may progressively recruit secondary pathways over several cycles. Operational screening should therefore evaluate injection performance together with gas breakthrough, liquid production, pressure communication, and the evolution of contacted and recoverable gas-accessible pore volume. The channel-dominated and balanced-expansion responses are treated here as phenomenological end members rather than universal reservoir or permeability classes; current evidence is insufficient to define unique permeability, pore-size, or capillary-threshold criteria that separate them.

3.4 Effect of injected-gas properties

Injected-gas composition controls gas density and viscosity, gas-oil interfacial properties, solubility, phase behavior, and compositional mass transfer. Nitrogen is convenient for laboratory experiments but does not reproduce hydrocarbon-gas dissolution into oil or extraction of light hydrocarbon components. In matched long-core tests, methane-rich hydrocarbon gas produced stronger liquid mobilization and a more extensively developed gas-flow network than nitrogen under the tested conditions (Zhang et al., 2026c). HPHT micromodel observations are mechanistically consistent with this response, showing gas dissolution, oil swelling, viscosity reduction, and fluid redistribution during capillary displacement (Zhang et al., 2026b).

These comparisons do not establish a universal ranking

Tab. 3 Representative evidence used to build the multiscale synthesis of oil-reservoir conversion to UGS

Reference	System / evidence scale	Observation used in this review	Role in the synthesis
De Kok et al. (2008)	Fractured oil reservoir; engineering study	Storage and oil recovery are coupled by fracture-matrix exchange and flow architecture.	Field-scale heterogeneity and pathway control
Bontemps et al. (2011)	Converted oil field; field case	Demonstrates practical conversion of a complex former oil field to UGS.	Field precedent for oil-reservoir conversion
Eren and Polat (2020)	Reservoir simulation; well configuration	Well architecture influences gas storage performance and oil recovery.	Completion and well-placement effects
Shi et al. (2012, 2013)	Water-invaded UGS; physical/pore-scale studies	Cyclic gas-water flow reorganizes water distribution and gas connectivity.	Analogue for water return and aquifer coupling
Wang et al. (2022)	Sandstone UGS; three-phase hysteresis	Hysteresis changes predicted injection-withdrawal response in high-intensity cycling.	Constitutive basis for cyclic flow functions
Zhang et al. (2022); Tang et al. (2025)	Oil-reservoir conversion; cyclic experiments	Multi-cycle injection-withdrawal changes multiphase-flow response, phase distribution, and accessible storage volume.	Independent support for progressive conversion
Zhang et al. (2026a)	Oil-reservoir UGS; cyclic core experiment	Storage capacity and flow response continue to evolve across repeated cycles.	Direct evidence for cycle-dependent pore-space release
Zhang et al. (2026a)	HPHT micromodel; hydrocarbon gas-oil-water	Preferential invasion, oil remobilization, trapping, and pathway loss/reconnection are directly visualized.	Pore-scale mechanism for hysteresis and remobilization
Zhang et al. (2026c)	Long-core cyclic injection-withdrawal	Rock/fluid conditions produce different modes of storage-space development and gas-liquid reorganization.	Direct evidence for observed channel-dominated and balanced-expansion end-member responses in the tested long-core systems
Zheng et al. (2026)	Water-invaded gas-reservoir UGS; cyclic experiment	Repeated cycling mobilizes retained water and reorganizes gas-water flow.	Comparison with water-invaded gas storage
Wei et al. (2026)	Reservoir-scale capacity evaluation	Effective capacity depends on dynamically swept and gas-accessible volume rather than nominal pore volume alone.	Reservoir-scale translation of dynamic capacity

of injected gases and do not demonstrate fully miscible displacement. Gas-oil phase behavior depends on oil composition, gas composition, pressure, temperature, and contact history. They do show that injected-gas identity cannot be treated as a minor experimental detail where compositional interaction controls liquid mobilization or produced-gas quality. Experiments intended for field transfer should therefore use reservoir-representative gas composition and pressure-temperature paths whenever practicable, supported by pressure-volume-temperature (PVT) measurements when compositional effects are expected to be important..

3.5 Reservoir heterogeneity, gravity, and well configuration

At field scale, dynamic conversion becomes a coupled areal/vertical sweep and pressure-communication problem. Stratification, faults, fractures, anisotropy, and completion architecture determine whether pore-scale preferential invasion develops into reservoir-scale flow channeling. Buoyancy drives gas toward structural highs and upper high-mobility intervals, whereas water tends to reoccupy lower intervals during withdrawal. In fractured reservoirs, pressure may communicate rapidly through fractures while matrix blocks retain substantial oil and water; pressure communication can therefore precede comparable release of matrix pore volume (De Kok et al., 2008; Bontemps et al., 2011).

Well architecture controls how strongly these geological tendencies are expressed. Horizontal wells, selective completions, or interval control can broaden injection and withdrawal, whereas poorly placed completions may reinforce dominant high-permeability paths (Eren and Polat, 2020). Storage-space development is therefore a coupled response of geology, gravity, completion design, fluids, aquifer support, and pressure-rate history. Reservoir simulation is most informative when

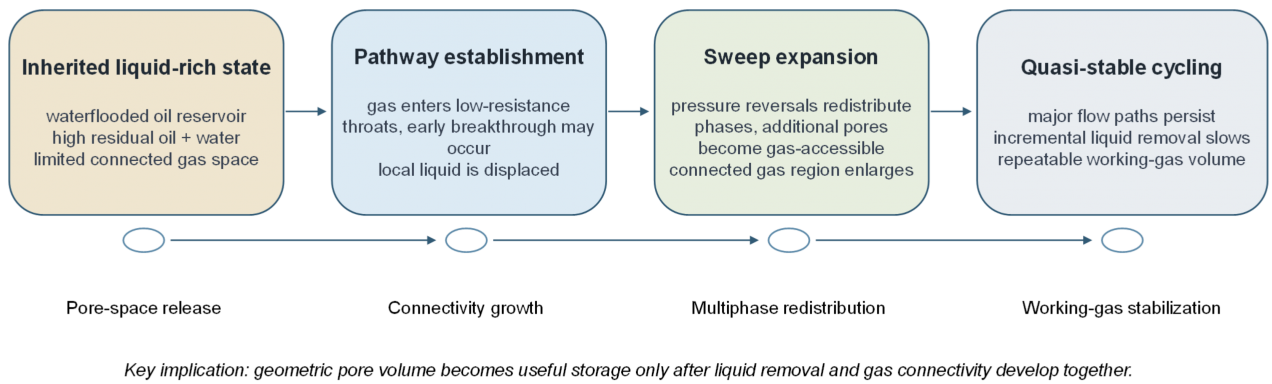

Fig. 2 Conceptual stages of working-gas-space reconstruction during cyclic injection-withdrawal

SCAL-derived saturation functions constrain local mobility and the model resolves gas saturation, liquid production, pressure communication, and water influx.

4 Cyclic multiphase flow and relative-permeability hysteresis

4.1 Why saturation alone is not enough

Multiphase Darcy flow requires saturation-dependent relative permeability and capillary pressure as constitutive closure relations. For phase i, mobility scales with relative permeability divided by viscosity ($k_r i/\mu_i$); consequently, a change in gas saturation does not map uniquely to a change in gas-flow capacity. UGS is intrinsically history dependent because injection and withdrawal repeatedly reverse the direction of saturation change. The same average gas saturation can therefore correspond to markedly different gas-phase connectivity, relative permeability, and pressure response during drainage, imbibition, shut-in redistribution, and reinjection.

During drainage, gas may establish a spanning network through pore bodies and connected throats; during withdrawal, wetting-phase imbibition and snap-off can fragment that network into disconnected ganglia. Oil may remain hydraulically connected through films after bulk oil saturation has declined, whereas water can re-enter through corners and smaller throats. These distinct phase topologies can exhibit markedly different conductivities at similar bulk saturations. Hysteresis is therefore not merely a saturation-memory effect; it reflects history-dependent changes in phase topology, trapping, and hydraulic connectivity (Blunt, 2017; DiCarlo et al., 2000; Oak et al., 1990; Scanziani et al., 2020).

Classical hysteresis models already capture part of this history. Land (1968) related residual nonwetting-phase saturation to the maximum saturation reached during drainage; Killough (1976) and Carlson (1981) provided practical scanning-curve procedures for reservoir simulation; Parker and Lenhard (1987) and Lenhard and Parker (1987) coupled hysteretic capillary-pressure and permeability-saturation behavior; and Larsen and Skauge (1998) explicitly considered cycle-dependent relative permeability. Their strength is that they compress a complicated saturation history into a tractable set of state variables.

For converted oil-reservoir UGS, the unresolved constitutive question is whether repeated cycling merely generates scanning paths within fixed drainage/imbibition bounding curves or progressively conditions the bounding curves themselves as retained liquids are mobilized. Cyclic storage and WAG studies confirm within-cycle hysteresis and suggest possible longer-term conditioning (Shahverdi and Sohrabi, 2015; Wang et al., 2022). The latter should presently be treated as a testable hypothesis rather than a universal property, particularly during early cycles when the inherited waterflooded saturation field evolves most rapidly.

4.2 Residual trapping and scanning behavior

Residual gas trapping is well documented in CO_2-brine systems because immobilized CO_2 contributes to secure geological storage. These studies show that trapping depends on maximum drainage saturation, pore structure, wettability, and capillary number, and that hysteretic relative permeability can materially alter plume-scale behavior (Juanes et al., 2006; Krevor et al., 2012, 2015; Akbarabadi and Piri, 2013; Ruprecht et al., 2014). Natural-gas UGS involves the same capillary trapping physics but a different operational objective: gas immobilized after withdrawal may no longer contribute to recoverable working gas.

Residual gas has a more complex interpretation in oil-reservoir UGS because the oil phase introduces additional mechanisms for cluster isolation and reconnection. Water re-imbibition can trap gas, oil or mixed-wet films can hydraulically separate clusters, and subsequent gas injection can reconnect part of the residual phase. Some immobile gas may effectively contribute to cushion-gas inventory and facilitate re-establishment of gas pathways, whereas another fraction remains unavailable to the working-gas cycle. Spatial distribution and connectivity are therefore more informative than core-averaged residual gas saturation alone.

Withdrawal deserves particular attention because it is not simply the reverse of gas injection. Falling pressure promotes wetting-phase re-entry, changes local capillary thresholds, and can narrow or break gas pathways. Flow reversal also changes interfacial shear on oil and water films. When injection resumes, some trapped gas reconnects and some clusters remain bypassed. A model intended for multi-cycle prediction must therefore reproduce not only residual saturation, but also the rate at which connected gas pathways are lost and reestablished.

4.3 Cycle-conditioned relative-permeability and capillary-pressure functions

Repeated SCAL under reservoir pressure and temperature is demanding, so reservoir models commonly assign one set of saturation functions to each rock type and use hysteresis scanning rules to represent reversals. During oil-reservoir conversion, however, a single fixed set may not represent first gas injection, early storage cycles, and mature cycling if progressive liquid drainage changes residual saturations, the mobile gas-saturation interval, or endpoint mobility.

Three levels of history dependence should be separated. Within-cycle hysteresis describes drainage-imbibition scanning around a given set of bounding curves. Between-cycle conditioning denotes a possible systematic change in endpoints, mobile saturation ranges, or curve shape after completed cycles. The longest time scale is the transition from the inherited waterflooded state to a mature cyclic storage state. Existing hysteresis algorithms are well developed for the first level, whereas the latter two remain sparsely constrained by direct three-phase measurements.

Changes in saturation range and endpoint mobility should not be collapsed into a single empirical cycle factor. A reduction in terminal liquid saturation mainly increases the pore volume available to gas; a higher gas relative-permeability endpoint mainly increases gas mobility and withdrawal deliverability at a given saturation. Working-gas capacity and well deliverability can therefore evolve at different rates and should be calibrated against different observables.

Any cycle-conditioned formulation should be built around measurable state variables such as maximum gas saturation, residual liquid saturation, reversal saturation, connected gas fraction, cumulative liquid production, or saturation-path extrema. Added state variables should first be tested against fixed-bounding-curve hysteresis and conventional scanning models at plug or core scale before they are introduced into field simulation; otherwise, improved history matching may simply reflect additional parameter freedom rather than improved physics.

5 Pore-scale gas-oil-water reorganization mechanisms

5.1 Preferential invasion and intermittent pathway growth

Gas entry is the first pore-scale step in storage-space reconstruction. Because local capillary entry pressure varies among throats, invasion proceeds by intermittent events rather than as a smooth front. Haines jumps and preferential invasion of larger or better-connected throats are well established (Berg et al., 2013; Blunt et al., 2013), and cyclic WAG/storage studies show strong path dependence (Sohrabi et al., 2004; Chowdhury et al., 2023; Gao et al., 2023). HPHT micromodels likewise show gas occupying favorable pathways while substantial oil and water remain in adjacent pores (Zhang et al., 2026b).

A first spanning gas path should not be mistaken for complete mobilization of the surrounding pore space. Once established, that path lowers resistance to subsequent gas throughput and can dominate measured injectivity. At the same time, it diverts pressure gradients away from neighboring liquid-rich regions and encourages bypassing. This pore-scale behavior provides a direct mechanistic counterpart to the channel-dominated response observed in highly connected long-core systems.

Whether invasion remains selective or becomes distributed depends on capillary-viscous balance and mobility ratio. Increasing injection rate may exceed additional entry thresholds but can also accelerate preferential breakthrough or viscous fingering. Capillary-number and mobility-ratio effects are therefore relevant to UGS pressure-rate design (Fulcher et al., 1985; Buckley and Leverett, 1942). The useful operating point is not necessarily maximum rate, but a pressure-rate path that enlarges connected gas access without excessive channeling or local overpressure.

5.2 Oil films, ganglia, and remobilization

Waterflooded residual oil occupies several pore-scale configurations: isolated ganglia, dead-end pores, wall films, corners, and locally connected layers. Their abundance and mobility depend strongly on wettability and pore geometry (Morrow, 1990; Sohrabi et al., 2004; Gao et al., 2022; Scanziani et al., 2020). These configurations do not respond equally to gas invasion. A large ganglion may require a substantial pressure gradient to move, whereas a thin oil film can remain connected and transport mass even when bulk oil saturation is low.

Hydrocarbon gas introduces a compositional mechanism in addition to capillary displacement. At reservoir pressure and temperature, gas may dissolve into oil, causing swelling and viscosity reduction, while lighter oil components may partition into the gas. High-pressure micromodel experiments on oil-reservoir UGS have observed local oil swelling and enhanced oil mobility during sustained gas contact (Zhang et al., 2026b). Gas-EOR studies provide broader support for the importance of pressure- and composition-dependent gas-oil interaction, although the magnitude and even the dominant mechanism vary among fluid systems (Jerauld, 1998; Ding et al., 2017; Gbadamosi et al., 2018). For storage conversion, remobilized oil has both a benefit and a cost. Moving liquid out of the developing gas zone can unlock additional pore volume, but the same process can create oil banks, increase liquid loading near wells, and alter produced-gas composition. A model may therefore reproduce reservoir pressure while still misrepresenting the rate at which gas-accessible space develops if gas-oil mass transfer and liquid redistribution are oversimplified.

5.3 Withdrawal, snap-off, and connectivity loss

Withdrawal reorganizes the pore network again. As pressure falls, gas volume decreases and local capillary balance shifts. Water can advance along corners or films, bridge throats, and snap off gas; oil films can thicken, thin, or detach under reversed interfacial shear. Direct high-pressure visualization shows that some pathways formed during injection partially collapse during withdrawal, leaving residual gas clusters and a different connectivity map for the next cycle (Zhang et al., 2026b).

This connectivity loss helps explain why deliverability can fall even when average gas saturation remains relatively high. A smaller connected cross-section is enough to reduce gas mobility. Conversely, residual gas occupying strategically important throats can shorten the distance required for reconnection during the next injection. Whether trapped gas is helpful cushion inventory or lost working gas therefore depends on where it sits in the network, not only on how much of it remains.

Three-dimensional synchrotron and micro-CT studies support this topological interpretation. In mixed-wet media, flow can persist through layers and films that simple pore-filling rules do not represent, and double-displacement events can rearrange two interfaces in a single local process (Scanziani et al., 2020; Razak et al., 2021; Noiriel and Renard, 2022). Two-dimensional micromodels cannot reproduce full three-dimensional connectivity, but they resolve rapid invasion and film motion that may be missed between tomographic scans. The two methods therefore answer different parts of the same question and are most useful when their observations are interpreted together.

5.4 Pore structure and fluid properties act together

Rock structure and fluid properties act jointly throughout conversion. Pore-throat size and connectivity control capillary entry-pressure distribution and pathway selectivity; wettability controls phase occupancy of surfaces, corners, and pore centers; oil viscosity governs liquid redistribution; and interfacial tension and pressure determine capillary number and influence gas-oil phase behavior. Consequently, the same nominal injection rate can correspond to different capillary numbers, mobility ratios, and saturation paths in different reservoir rock-fluid systems.

Absolute permeability alone is therefore a weak screening variable for dynamic convertibility. A high-permeability reservoir with strong vertical contrast, preferential fractures, or viscous residual oil may channel more severely than a moderately permeable but better distributed pore network. Laboratory comparisons should preserve the representative rock-fluid pair where possible and report wettability, pressure-temperature path, viscosity ratio, interfacial tension or capillary-number range, and saturation history rather than treating permeability as the sole descriptor.

6 Cross-scale translation from fluid mobilization to storage performance

6.1 From pore topology to relative permeability

The first upscaling step is from pore configuration to continuum saturation functions. Invasion, snap-off, film flow, trapping, and reconnection determine which portions of each phase contribute to flow. Relative permeability is an effective closure integrating connectivity, saturation distribution, wettability, and viscous-capillary interactions (Brooks and Corey, 1964; Mualem, 1976; van Genuchten, 1980; Dullien, 1992). Reconnection of a small gas volume across critical throats can therefore increase effective gas mobility much more than the corresponding change in bulk gas saturation.

Pore-scale experiments should therefore be interpreted in terms of hydraulic connectivity as well as saturation. Cluster connectivity, spanning pathways, interfacial area, cluster-size distribution, and topological descriptors can explain mobility changes that bulk saturation alone cannot. Dynamic micro-CT and image-based modeling increasingly make such measurements feasible (Wang et al., 2021; Li et al., 2023), but upscaling requires matched rock-scale flow measurements under comparable pressure, wettability, and saturation-history conditions.

6.2 From relative permeability to injectivity and deliverability

At reservoir scale, relative permeability controls multiphase mobility and the pressure gradient required for a given rate. Near-well gas mobility can rise after a connected path forms while the far field remains liquid rich; during withdrawal, wetting-phase return and gas trapping can lower gas relative permeability and deliverability. Field-scale well performance also depends on gas PVT, completion and skin, wellbore hydraulics, and high-rate non-Darcy effects; these should not be absorbed incorrectly into relative-permeability calibration.

Injectivity, withdrawal deliverability, and working-gas capacity should therefore be evaluated together but not treated as interchangeable metrics. Injectivity probes the pressure-rate response during gas entry; deliverability measures sustainable withdrawal at acceptable drawdown; and field WGV is the surface-standard gas inventory cycled between lower and upper operating pressure limits. All three depend on the evolving multiphase saturation field, but they respond differently to relative permeability, gas PVT, accessible pore volume, aquifer influx, and well/completion effects.

6.3 From liquid-displacement efficiency and gas sweep to effective storage capacity

Two processes determine how much geological pore volume participates in cyclic storage: liquid release within contacted rock and reservoir-scale gas sweep/connectivity. Zhang et al. (2026a) defined liquid-displacement efficiency (LDE) as displaced oil plus formation water normalized by movable-oil volume in their HPHT long-core experiment. LDE increased through the six cycles, with the largest incremental response reported by Cycle 3, whereas gas relative permeability continued to improve and reached 56.4% by Cycle 6. This offset shows that liquid drainage and gas-flow capacity do not necessarily peak together.

Zhang et al. (2026c) reached the same conclusion from long-core comparisons: under the tested stepwise pressure-varying scheme, cyclic injection-withdrawal increased oil-displacement efficiency from 68.5% to 81.8% and LDE from 40.1% to 56.3% relative to one-way gas flooding. Zhang et al. (2026b) provides the pore-scale explanation: waterflooding leaves oil films and ganglia; gas injection forms preferential pathways by intermittent invasion and Haines jumps and can remobilize oil through gas dissolution and swelling; withdrawal promotes water reimbibition, pathway collapse, and residual-gas trapping.

Accordingly, displacement efficiency should not be used as a stand-alone storage metric. Evaluate (i) liquid drainage with ODE/LDE and liquid production, (ii) gas-space activation with gas saturation, gas relative permeability, and connectivity, and

(iii) cyclic recoverability with gas sweep, pressure response, connected gas inventory, and WGV/material balance. Tab. 4 summarizes the indicators and limitations. This is an evidence hierarchy, not a calibrated equation; the cited experiments do not establish a universal field-scale conversion coefficient. Reservoir-scale capacity still requires PVT, pressure limits, aquifer response, and material balance (Wei et al., 2026).

6.4 Cross-scale framework and feedbacks

The progressive storage-space mobilization framework established from long-core cyclic injection-withdrawal experiments provides a process-level description of oil-reservoir UGS conversion: cyclic pressure variation redistributes trapped liquids, expands gas invasion, and progressively develops gas-phase connectivity (Zhang et al., 2026c). This experimentally based process forms the left-hand foundation of the cross-scale synthesis in Fig. 3. The review synthesis extends that process across scales. Pore structure, wettability, fluid properties, and operating history control three-phase topology and connectivity; their hydraulic consequences appear as relative-permeability/capillary-pressure hysteresis and, potentially, between-cycle conditioning of the bounding saturation functions. These constitutive relations control liquid mobilization, gas sweep, pressure redistribution, and pathway competition, which ultimately govern injectivity, withdrawal deliverability, working-gas capacity, and produced-fluid behavior. The sequence is not one-way. Pressure and rate alter saturation topology; topology changes phase mobility; mobility redistributes pressure and sweep and conditions the next cycle. Pressure response, well rates, produced liquids, gas-water ratio, and gas composition can therefore constrain reservoir-model updates and subsequent pressure-rate strategy. The feedback arrow in Fig. 3 is conceptual, not a calibrated constitutive law: field surveillance cannot uniquely determine pore-scale mechanisms or saturation functions without laboratory and history-matching constraints.

6.5 Scaling limits and evidence hierarchy

No single experimental scale reproduces the complete conversion process. Micromodels resolve rapid interfacial events and pore-scale displacement but simplify three-dimensional geometry and connectivity; plugs constrain constitutive saturation functions but suppress field-scale saturation gradients; long cores reveal breakthrough, pressure redistribution, and flow-path competition but sample only limited heterogeneity; and reservoir simulation restores field geometry and well configuration while inheriting uncertainty in saturation functions, PVT, aquifer behavior, geomechanics, and unresolved sub-grid structure.

Evidence should therefore be weighted according to the process each scale can resolve: imaging is strongest for mechanism identification, SCAL for constitutive functions, long-core experiments for coupled rock-fluid response and operating schedules, and field surveillance for storage-scale relevance. Convergent evidence across scales is more persuasive than a close match at any single scale. Laboratory trends should not be converted directly into field-scale multipliers without an explicit constitutive or upscaling relationship, and a reservoir history match remains non-unique and does not by itself validate a specific pore-scale mechanism.

7 Engineering implications and research priorities

7.1 Dynamic convertibility as a screening criterion

Conventional site screening emphasizes structural closure, seal integrity, pore volume, depth, pressure, permeability, well condition, and surface infrastructure. High-water-cut oil reservoirs require an additional multiphase-flow criterion: how readily can liquid-occupied pore volume be converted into a hydraulically connected gas system within a realistic operating-pressure window, rate range, and number of cycles? This review terms that property dynamic convertibility. It is an integrated screening concept rather than a single intrinsic rock property.

Dynamic convertibility depends on pore-throat connectivity, vertical and areal heterogeneity, residual-liquid distribution, capillary entry pressure, wettability, aquifer strength, gas-oil interaction, well configuration, and the admissible pressure window. A large but compartmentalized reservoir may yield less effective working-gas space than a smaller reservoir with favorable connectivity and manageable water influx. Screening should therefore combine static geology and containment with evidence on liquid mobilization, gas sweep, hysteresis, pressure communication, and well integrity. Recent oil-reservoir UGS studies have also proposed water-drive efficiency and sweep efficiency as conversion-specific site-screening indicators (Yu et al., 2026). Within the present framework, these indices constrain dynamic convertibility by characterizing the inherited waterflood state and the fraction of reservoir volume that can subsequently be contacted by storage gas.

7.2 Stage-dependent operating strategy

A single pressure-rate policy is unlikely to remain optimal from initial conversion to mature cyclic operation. During flow-path establishment, the priority is to develop gas-phase continuity without excessive bottomhole pressure or premature gas breakthrough. During sweep expansion, saturation excursion and the operating-pressure window may be increased only within caprock, fault, well-integrity, and geomechanical constraints, with surveillance for water return and preferential channeling. Once cyclic behavior becomes repeatable, the operating objective shifts toward stable withdrawal deliverability, working-gas recovery, and control of produced water and oil. At reservoir scale, progressive gas-phase connectivity may ultimately manifest as formation and stabilization of a secondary gas cap, particularly where buoyancy segregation is pronounced (Yu et al., 2026). Its development should be evaluated jointly with liquid drainage, vertical gas sweep, pressure communication, and allowable operating pressure rather than as a volumetric gas-inventory problem alone.

Injection rate should therefore be evaluated by its effects on both pressure response and the evolving connected gas volume, rather than by maximum sustainable rate alone. A higher rate may overcome local capillary entry pressures, but it can also reinforce preferential channels, elevate near-well pressure, and

Tab. 4 Experimental indicators for evaluating liquid-drainage efficiency, gas-space activation, and working-gas-space development during oil-reservoir conversion to UGS

Indicator	Direct evidence in the cited studies	Storage interpretation	Main limitation
Oil-displacement efficiency (ODE)	Zhang et al. (2026a,c): quantifies residual-oil mobilization; Zhang et al. (2026c) reports 68.5% to 81.8% under the tested cyclic scheme.	Measures oil drainage from contacted rock and helps track release of oil-occupied pore volume.	Does not include water drainage, gas sweep, or cyclic gas connectivity.
Liquid-displacement efficiency (LDE)	Zhang et al. (2026a): defined for displaced oil plus formation water; Zhang et al. (2026c) reports 40.1% to 56.3% under the tested cyclic scheme.	Core-scale indicator of liquid-occupied pore-space liberation.	Normalization is experiment-specific; LDE is not field WGV.
Incremental liquid displacement by cycle	Zhang et al. (2026a): the largest incremental LDE response was reported by Cycle 3, after which the rate of increase slowed.	Tracks when active liquid drainage is strongest and when marginal pore-space release begins to diminish.	Cycle number is not an independent control because the tested pressure window also changed between cycles.
Gas saturation and gas relative permeability	Zhang et al. (2026a,c): used with displacement efficiencies to track gas occupation and mobility; k_rg reached 56.4% by Cycle 6 in Zhang et al. (2026a).	Constrains gas-space activation and flow capability after liquid drainage.	Core-scale mobility does not quantify reservoir-wide areal or vertical sweep.
HPHT pore-scale visualization	Zhang et al. (2026b): oil films/ganglia, Haines-jump invasion, gas-oil dissolution and swelling, withdrawal-induced pathway collapse and gas trapping.	Explains why liquid displacement, gas connectivity, and hysteresis are coupled but not equivalent.	Two-dimensional micromodel observations are mechanistic, not direct field-scale efficiency measurements

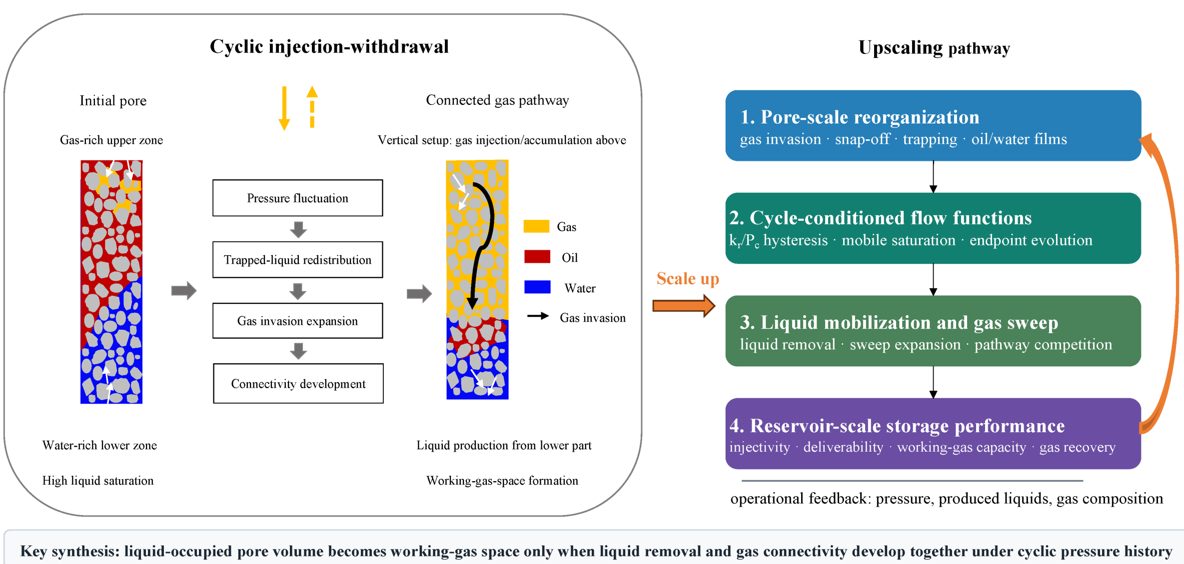

Fig. 3 Cross-scale framework for dynamic working-gas-space reconstruction in oil-reservoir UGS

intensify high-rate non-Darcy pressure losses at field scale. The relevant design variable is the pressure-rate trajectory that maximizes growth of recoverable gas-accessible pore volume while remaining within containment and well-integrity limits and preserving acceptable sweep and withdrawal performance.

Experimental results support tracking liquid drainage incrementally. Zhang et al. (2026a) reported the strongest incremental LDE response by Cycle 3 while gas relative permeability improved through Cycle 6; Zhang et al. (2026c) varied the pressure window stepwise. Marginal LDE and gas mobility should therefore be interpreted together rather than using cycle count alone.

Tab. 5 Cross-scale observables and their engineering interpretation in high-water-cut oil-reservoir UGS

Scale	Main observables	Information resolved	Engineering use
Pore	Cluster connectivity, wetting films, snap-off, Haines jumps, interfacial area	Local invasion, trapping, reconnection, and liquid remobilization	Mechanistic interpretation of hysteresis and connectivity loss
Plug/SCAL	Relative-permeability/capillary-pressure curves, endpoints, residual saturations, scanning curves	Phase mobility, trapping, and saturation-history dependence	Simulator saturation functions and hysteresis calibration
Long core	Pressure drop, gas saturation, produced liquids, gas breakthrough	Storage-space mobilization, saturation redistribution, and pathway competition	Rock-fluid comparison and operating-schedule testing
Reservoir	Gas-saturation distribution, pressure, gas inventory/WGV, gas-water ratio (GWR), liquid production	Areal/vertical sweep, gas connectivity, aquifer interaction, pressure communication	Capacity and injectivity/deliverability forecast
Field surveillance	Pressure-transient analysis, production logging (PLT), tracers, fluid composition, time-lapse saturation monitoring	Flow-path communication, interval contribution, and saturation redistribution	Model discrimination/history matching, operating optimization, and uncertainty reduction

Tab. 6 Main controls, risks, and preferred diagnostic responses

Control	Potential benefit	Main risk if unmanaged	Useful diagnostics
High permeability / connectivity	High injectivity and rapid pressure communication	Early gas breakthrough, channeling, and uneven sweep	Pressure-transient analysis, tracer breakthrough, PLT
Moderate/fine pore throats	Potential for distributed progressive gas invasion after local entry thresholds are exceeded	High capillary entry pressure and delayed gas-path establishment	Multi-rate injection, MICP/capillary testing, SCAL
Strong aquifer	Pressure support and reduced depletion drawdown	Water return, gas relative-permeability loss, reduced deliverability	Water production/GWR, pressure history, saturation monitoring
Residual oil	Possible remobilization and release of liquid-occupied pore volume	Pore-volume occupation, liquid banks, produced-gas contamination	Produced-fluid composition, PVT, cyclic core flooding
Wide pressure cycling	Larger saturation excursion and possible additional liquid mobilization	Integrity risk, water return, and additional gas trapping during reversal	Pressure/geomechanical surveillance, well integrity, cyclic SCAL
Hydrocarbon-gas interaction	Oil swelling/viscosity reduction and enhanced liquid mobilization	Compositional change, gas-quality change, phase-behavior uncertainty	PVT/phase-behavior tests, compositional sampling, HPHT visualization

7.3 Cycle-conditioned three-phase flow functions

The largest constitutive uncertainty is whether repeated gas-oil-water cycling modifies the bounding relative-permeability and capillary-pressure functions in addition to generating conventional scanning hysteresis. Most reservoir simulators can represent drainage-imbibition reversals, but few datasets establish whether endpoints, residual saturations, and mobile saturation intervals remain stationary as a waterflooded oil reservoir evolves toward mature UGS operation. Multi-cycle measurements at reservoir pressure and temperature are therefore required, together with independent saturation measurements and material-balance closure.

Three-phase measurements require particular attention because separate two-phase relative-permeability curves do not uniquely determine three-phase connectivity or constitutive closure. Where full three-phase SCAL is impractical, gas-oil, gas-water, and oil-water measurements should be integrated with pore-scale observations and validated against long-core cycling. Apparatus artifacts, capillary-end effects, evaporation or compositional change, incomplete steady state, and saturation-measurement uncertainty must be distinguished from genuine between-cycle conditioning before endpoint evolution is inferred.

7.4 Upscaling pore-scale hysteresis

Pore-scale imaging can resolve trapping, film flow, and reconnection, but field models cannot track individual clusters. Upscaling should therefore target a compact set of state variables that preserve hydraulic consequences, such as maximum gas saturation, connected gas fraction, residual liquid saturation, reversal saturation, and cumulative liquid production, and judge them by their ability to predict measured mobility.

A productive route is to pair imaging and SCAL on matched rock-fluid systems: quantify connectivity through a controlled cycle, measure the corresponding relative permeability, derive a compact state relation, and test it in a long-core or sector model. This turns pore-scale observations from qualitative explanation into constitutive constraints.

7.5 Gas-oil mass transfer and produced-gas quality

Gas dissolution, oil swelling, and vaporization/extraction of light hydrocarbons can occur under reservoir conditions, yet many conversion simulations still use simplified black-oil descriptions or inert laboratory gases. Compositional effects can alter oil viscosity and swelling, gas density and viscosity, interfacial behavior, phase partitioning, and produced-gas composition. Their importance is reservoir specific, so the need for compositional simulation should be established from PVT and phase-behavior evidence rather than assumed a priori.

PVT measurements, phase-behavior tests, and cyclic displacement should therefore be interpreted in a common material-balance framework. A process that releases pore volume through oil swelling, viscosity reduction, or component transfer may improve gas access while simultaneously increasing surface-separation requirements or changing gas calorific value. Storage performance, produced-gas quality, and any incremental oil recovery should therefore be evaluated together rather than as independent outcomes.

7.6 Aquifer coupling and water return

Aquifer influx provides pressure support but competes directly with gas for connected pore volume. During withdrawal, water can re-enter gas-bearing intervals, reduce gas relative permeability, increase near-well liquid loading, and impair deliverability. Repeated cycling may either stabilize a gas-water transition zone or promote progressive water encroachment, depending on pressure history, aquifer strength, vertical communication, and well completion. Experience from water-invaded gas-reservoir UGS therefore provides an important mechanistic analogue for converted oil reservoirs (Shi et al., 2012, 2013; Zheng et al., 2026).

The key engineering threshold is the point at which aquifer support changes from beneficial pressure maintenance to a constraint on participating gas volume and withdrawal deliverability. Resolving that threshold requires coupled reservoir-aquifer models calibrated against multi-cycle pressure, water production, gas-water ratio, and saturation indicators rather than a single static estimate of aquifer strength.

7.7 Channel-dominated versus balanced-expansion behavior

The channel-dominated/balanced-expansion concept should be tested across a broader range of rock types, fluid systems, and reservoir architectures. Current evidence supports these responses as mechanistic end members rather than universal reservoir classes. Highly connected systems can establish gas pathways rapidly but may subsequently concentrate flow into a small number of dominant channels; stronger capillary constraints may delay initial connectivity while enabling continued recruitment of secondary pathways during later cycles. However, available evidence does not support a unique permeability, pore-throat, or capillary-number threshold separating the two behaviors. Fractured reservoirs, strongly layered systems, anisotropic formations, and reservoirs with active aquifers may exhibit intermediate or additional responses beyond the present two-end-member description.

A useful field indicator should combine injectivity with independent evidence of sweep efficiency and flow-path distribution. High injectivity accompanied by early tracer breakthrough, strongly localized production-logging response, or persistent interval dominance may indicate channelized flow rather than efficient storage-space development. Pressure-transient analysis, production logging, tracers, produced-fluid composition, and time-lapse saturation monitoring can help distinguish a broadly connected productive volume from a narrow high-rate pathway.

7.8 Field calibration and uncertainty

The largest remaining uncertainty lies in translating laboratory cycling behavior to field-scale storage operation. Laboratory systems reproduce selected force balances and fluid interactions, whereas field response additionally reflects kilometre-scale heterogeneity, well patterns, gravity segregation, long shut-ins, high-rate non-Darcy effects, compositional processes, aquifer support, geomechanics, and surveillance uncertainty. Field history matching is therefore inherently non-unique unless the monitoring data are selected to discriminate among competing flow mechanisms.

Field pilots should therefore be designed to discriminate among mechanisms rather than merely demonstrate injectivity. Baseline saturation and pressure distributions should be reconstructed from development history; early storage cycles should integrate pressure-rate data with production logging, produced-fluid composition, tracers, and saturation surveillance where feasible; and the reservoir model should be updated as cycle data accumulate. The most informative measurements are those that distinguish responses caused by net liquid drainage, gas-path reconnection, aquifer movement, fluid-property changes, well skin or non-Darcy effects, and pressure communication through high-permeability features.

8 Conclusions

High-water-cut oil reservoirs should be treated as a distinct UGS conversion system rather than simply as depleted gas reservoirs with a higher liquid saturation. Geological pore volume is known at the start of conversion, but the fraction that becomes gas-accessible, hydraulically connected, and cyclically recoverable is not. Initial gas injection establishes preferential pathways, whereas withdrawal and reinjection impose drainage-imbibition reversals that redistribute oil, water, and gas, mobilize part of the liquid-occupied pore volume, and repeatedly disconnect and reconnect gas pathways until a more reproducible cyclic saturation topology develops.

Three principal conclusions emerge. First, working-gas capacity is controlled jointly by local liquid release and reservoir-scale gas sweep/connectivity. Oil-displacement efficiency (ODE) and liquid-displacement efficiency (LDE) quantify liquid mobilization, but they must be interpreted together with gas saturation, gas relative permeability, and WGV/material balance because pore-volume liberation and gas-flow capacity can evolve at different rates. Second, trapping, film redistribution, wetting-phase return, and pathway reconnection generate pronounced hysteresis, whereas systematic between-cycle evolution of bounding-curve endpoints remains insufficiently constrained. Third, pore architecture, wettability, fluid properties, and operating history control phase topology; topology and saturation history determine relative permeability and capillary pressure; and these constitutive functions govern liquid mobilization, gas sweep, injectivity, withdrawal deliverability, and recoverable gas inventory.

Conversion design should target the development of hydraulically connected and repeatedly recoverable gas-storage space rather than maximum instantaneous injection rate or theoretical pore volume. Key unresolved issues include possible between-cycle conditioning of three-phase saturation functions, upscaling of phase connectivity and hysteresis, gas-oil compositional mass transfer, aquifer-driven water return, controls on channel-dominated versus distributed storage-space development, and calibration against multi-cycle field surveillance. Field response should subsequently inform the next-cycle pressure-rate strategy and reservoir-model update, enabling candidate reservoirs to be ranked by dynamic convertibility in addition to static storage potential.

Acknowledgements

This work was supported by the National Science and Technology Major Project (Grant No. 2025ZD1406800).

Conflict of interest

The authors declare no competing interest.

References

Akbarabadi M, Piri M. 2013. Relative permeability hysteresis and capillary trapping characteristics of supercritical CO_2/brine systems: An experimental study at reservoir conditions. *Advances in Water Resources*, **52**: 190-206. doi:10.1016/j.advwatres.2012.06.014.

Andrew M, Menke H, Blunt MJ, et al. 2015. The imaging of dynamic multiphase fluid flow using synchrotron-based X-ray microtomography at reservoir conditions. *Transport in Porous Media*, **110**(1): 1-24. doi:10.1007/s11242-015-0553-2.

Anikin OV, Derevyanko VK, Bolotov AV, et al. 2025. Gas enhanced oil recovery methods for offshore oilfields: Features, implementation, operational status. *Petroleum Research*, **10**(2): 404-415. doi:10.1016/j.ptlrs.2024.12.003.

Bakhshian S, Hosseini SA, Shokri N. 2019. Pore-scale characteristics of multiphase flow in heterogeneous porous media using the lattice Boltzmann method. *Scientific Reports*, **9**: 3377. doi:10.1038/s41598-019-39741-x.

Berg S, Ott H, Klapp SA, et al. 2013. Real-time 3D imaging of Haines jumps in porous media flow. *Proceedings of the National Academy of Sciences*, **110**(10): 3755-3759. doi:10.1073/pnas.1221373110.

Blunt MJ. 2000. An empirical model for three-phase relative permeability. *SPE Journal*, **5**(4): 435-445. doi:10.2118/67950-PA.

Blunt MJ. 2001. Flow in porous media-pore-network models and multiphase flow. *Current Opinion in Colloid & Interface Science*, **6**(3): 197-207. doi:10.1016/S1359-0294(01)00084-X.

Blunt MJ. 2017. Multiphase Flow in Permeable Media: A Pore-Scale Perspective. Cambridge University Press, Cambridge. doi:10.1017/9781316145098.

Blunt MJ, Bijeljic B, Dong H, et al. 2013. Pore-scale imaging and modelling. *Advances in Water Resources*, **51**: 197-216. doi:10.1016/j.advwatres.2012.03.003.

Bontemps C, Egermann P, Foerster R, Gerken G. 2011. Reitbrook, a successful conversion of a former complex oil field into underground gas storage. 18th International Petroleum and Natural Gas Congress and Exhibition of Turkey. European Association of Geoscientists and Engineers, cp-377-00044. doi:10.3997/2214-4609-pdb.377.44.

Brooks RH, Corey AT. 1964. Hydraulic Properties of Porous Media. Colorado State University, Fort Collins, Hydrology Paper No. 3.

Buckley SE, Leverett MC. 1942. Mechanism of fluid displacement in sands. *Transactions of the AIME*, **146**(1): 107-116. doi:10.2118/942107-G.

California Geologic Energy Management Division (CalGEM). n.d. Aliso Canyon Storage Facility. California Department of Conservation. https://www.conservation.ca.gov/calgem/AlisoCanyon/Pages/AlisoCanyon.a (accessed 28 August 2026).

Carlson FM. 1981. Simulation of relative permeability hysteresis to the nonwetting phase. SPE-10157-MS, SPE Annual Technical Conference and Exhibition, San Antonio, Texas. doi:10.2118/10157-MS.

China News Service. 2024. China's first offshore gas storage facility officially put into operation. 27 November 2024. https://www.chinanews.com.cn/tp/2024/11-27/10326639.shtml (accessed 28 August 2026).

Chowdhury S, Rakesh M, Medhi S, et al. 2023. Three-phase fluid flow interaction at pore scale during water- and surfactant-alternating gas injection using carbon dioxide for geo-sequestration and enhanced oil recovery. *Energy & Fuels*, **37**(7): 5270-5290. doi:10.1021/acs.energyfuels.2c03982.

De Kok J, Ali A, Clemens T. 2008. Synergies of underground gas storage and enhanced oil recovery in a fractured reservoir. SPE Russian Petroleum Technology Conference, SPE-114658-MS. doi:10.2118/114658-MS.

DiCarlo DA, Sahni A, Blunt MJ. 2000. The effect of wettability on three-phase relative permeability. *Transport in Porous Media*, **39**(3): 347-366. doi:10.1023/A:1006653323374.

Ding GS, Li C, Wang JM, et al. 2015. The status quo and technical development direction of underground gas storages in China. *Natural Gas Industry B*, **2**(6): 535-541. doi:10.1016/j.ngib.2015.12.007.

Ding M, Yuan F, Wang Y, et al. 2017. Oil recovery from a CO_2 injection in heterogeneous reservoirs: The influence of permeability heterogeneity, CO_2-oil miscibility and injection pattern. *Journal of Natural Gas Science and Engineering*, **44**: 140-149. doi:10.1016/j.jngse.2017.04.015.

Dullien FAL. 1992. Porous Media: Fluid Transport and Pore Structure, 2nd ed. Academic Press, San Diego. doi:10.1016/C2009-0-26184-8.

Eren T, Polat C. 2020. Natural gas underground storage and oil recovery with horizontal wells. *Journal of Petroleum Science and Engineering*, **187**: 106753. doi:10.1016/j.petrol.2019.106753.

Evans DJ, Chadwick RA. 2009. Underground gas storage: An introduction and UK perspective. *Geological Society, London, Special Publications*, **313**: 1-11. doi:10.1144/sp313.1.

Fulcher RA Jr, Ertekin T, Stahl CD. 1985. Effect of capillary number and its constituents on two-phase relative permeability curves. *Journal of Petroleum Technology*, **37**(2): 249-260. doi:10.2118/12170-PA.

Gao G, Zhang Y, Yang Z, et al. 2025. Sealing integrity in faulted underground gas storage: A case study of the Nanpu-1 gas storage, Eastern China. *Energy Reports*, **13**: 1004-1013. doi:10.1016/j.egyr.2024.12.047.

Gao J, Kong D, Peng Y, et al. 2023. Pore-scale mechanisms and hysteresis effect during multi-cycle injection and production process in underground hydrogen storage reservoir. *Energy*, **283**: 129007. doi:10.1016/j.energy.2023.129007.

Gao Y, Xie X, Wang S, et al. 2022. Pore-scale experimental investigation of the remaining oil formation in water-wet, mixed-wet and oil-wet sandstone samples. *Journal of Petroleum Science and Engineering*, **216**: 110790. doi:10.1016/j.petrol.2022.110790.

Gbadamosi AO, Kiwalabye J, Junin R, et al. 2018. A review of gas enhanced oil recovery schemes used in the North Sea. *Journal of Petroleum Exploration and Production Technology*, **8**(4): 1373-1387. doi:10.1007/s13202-018-0451-6.

Hagoort J. 1988. Fundamentals of Gas Reservoir Engineering. Elsevier, Amsterdam. ISBN 978-0-444-42991-9.

He YT, Tian SC, Song XZ, et al. 2026. Experimental investigation of caprock wettability and helium-water interfacial tension: Implications for structural gas geostorage capacity estimation. *GeoStorage*, **2**(2): 98-105. doi:10.46690/gs.2026.02.01.

Honarpour MM, Koederitz LF, Harvey AH. 1986. Relative Permeability of Petroleum Reservoirs, 1st ed. CRC Press, Boca Raton. doi:10.1201/9781351076326.

IGU Storage Committee. 2025. Underground Gas Storage: A Critical Pillar for Energy Security. International Gas Union, 17 pp. https://www.datocms-assets.com/146580/1761301320-underground-gas-storage_report.pdf (accessed 28 August 2026).

Jerauld G. 1998. A case study in scaleup for multicontact miscible hydrocarbon gas injection. *SPE Reservoir Evaluation & Engineering*, **1**(6): 575-582. doi:10.2118/53006-PA.

Jiang CB, Tang SS, Wu MY, et al. 2026. Progress in energy storage of depleted oil and gas reservoirs: A perspective based on fluid migration. *GeoStorage*, **2**(2): 137-155. doi:10.46690/gs.2026.02.03.

Jiang T, Wang Z, Wang J. 2021. Integrated construction technology for natural gas gravity drive and underground gas storage. *Petroleum Exploration and Development*, **48**(5): 1227-1236. doi:10.1016/S1876-3804(21)60105-2.

Juanes R, Spiteri EJ, Orr FM Jr, et al. 2006. Impact of relative permeability hysteresis on geological CO_2 storage. *Water Resources Research*, **42**(12): W12418. doi:10.1029/2005WR004806.

Kanaani M, Sedaee B, Asadian-Pakfar M. 2022. Role of cushion gas on underground hydrogen storage in depleted oil reservoirs. *Journal of Energy Storage*, **45**: 103783. doi:10.1016/j.est.2021.103783.

Katz DL, Tek MR. 1981. Overview on underground storage of natural gas. *Journal of Petroleum Technology*, **33**(6): 943-951. doi:10.2118/9390-PA.

Killough JE. 1976. Reservoir simulation with history-dependent saturation functions. *SPE Journal*, **16**(1): 37-48. doi:10.2118/5106-PA.

Krevor S, Blunt MJ, Benson SM, et al. 2015. Capillary trapping for geologic carbon dioxide storage-from pore scale physics to field scale implications. *International Journal of Greenhouse Gas Control*, **40**: 221-237. doi:10.1016/j.ijggc.2015.04.006.

Krevor SCM, Pini R, Zuo L, et al. 2012. Relative permeability and trapping of CO_2 and water in sandstone rocks at reservoir conditions. *Water Resources Research*, **48**(2): W02532. doi:10.1029/2011WR010859.

Land CS. 1968. Calculation of imbibition relative permeability for two- and three-phase flow from rock properties. *SPE Journal*, **8**(2): 149-156. doi:10.2118/1942-PA.

Larsen JA, Skauge A. 1998. Methodology for numerical simulation with cycle-dependent relative permeabilities. *SPE Journal*, **3**(2): 163-173. doi:10.2118/38456-PA.

Lenhard RJ, Parker JC. 1987. A model for hysteretic constitutive relations governing multiphase flow: 2. Permeability-saturation relations. *Water Resources Research*, **23**(12): 2197-2206. doi:10.1029/WR023i012p02197.

Li M, Foroughi S, Zhao J, et al. 2023. Image-based pore-scale modelling of the effect of wettability on breakthrough capillary pressure in gas diffusion layers. *Journal of Power Sources*, **584**: 233539. doi:10.1016/j.jpowsour.2023.233539.

Liu JJ, Yang CH, Song R, et al. 2025. Advances of geological storage engineering and technology. *GeoStorage*, **1**(1): 1-26. doi:10.46690/gs.2025.01.01.

Lysyy M, Ersland G, Ferno M. 2022. Pore-scale dynamics for underground porous media hydrogen storage. *Advances in Water Resources*, **163**: 104167. doi:10.1016/j.advwatres.2022.104167.

Lysyy M, Ferno M, Ersland G. 2021. Seasonal hydrogen storage in a depleted oil and gas field. *International Journal of Hydrogen Energy*, **46**(49): 25160-25174. doi:10.1016/j.ijhydene.2021.05.030.

Morrow NR. 1990. Wettability and its effect on oil recovery. *Journal of Petroleum Technology*, **42**(12): 1476-1484. doi:10.2118/21621-PA.

Mualem Y. 1976. A new model for predicting the hydraulic conductivity of unsaturated porous media. *Water Resources Research*, **12**(3): 513-522. doi:10.1029/WR012i003p00513.

Noiriel C, Renard F. 2022. Four-dimensional X-ray micro-tomography imaging of dynamic processes in geosciences. *Comptes Rendus Geoscience*, **354**(G2): 255-280. doi:10.5802/crgeos.137.

Oak MJ, Baker LE, Thomas DC. 1990. Three-phase relative permeability of Berea sandstone. *Journal of Petroleum Technology*, **42**(8): 1054-1061. doi:10.2118/17370-PA.

Parker JC, Lenhard RJ. 1987. A model for hysteretic constitutive relations governing multiphase flow: 1. Saturation-pressure relations. *Water Resources Research*, **23**(12): 2187-2196. doi:10.1029/WR023i012p02187.

Perreaux M, Bontemps C, Egermann P. 2015. Reitbrook case study: Enhancing oil recovery through the underground gas storage activity. SPE Asia Pacific Enhanced Oil Recovery Conference, SPE-174647-MS. doi:10.2118/174647-MS.

Plaat H. 2009. Underground gas storage: Why and how. *Geological Society, London, Special Publications*, **313**: 25-37. doi:10.1144/SP313.4.

Razak WAW, Kechut NI, Andrews E, et al. 2021. 3D visualization of film flow during three-phase displacement in water-wet rocks via microtomography method. *Abu Dhabi International Petroleum Exhibition and Conference*, SPE-207460-MS. doi:10.2118/207460-MS.

Ruprecht C, Pini R, Falta R, et al. 2014. Hysteretic trapping and relative permeability of CO_2 in sandstone at reservoir conditions. *International Journal of Greenhouse Gas Control*, **27**: 15-27. doi:10.1016/j.ijggc.2014.05.003.

Scanziani A, Alhosani A, Lin Q, et al. 2020. In situ characterization of three-phase flow in mixed-wet porous media using synchrotron imaging. *Water Resources Research*, **56**(9): e2020WR027873. doi:10.1029/2020WR027873.

Shahverdi H, Sohrabi M. 2015. Modeling of cyclic hysteresis of three-phase relative permeability during water-alternating-gas injection. *SPE Journal*, **20**(1): 35-48. doi:10.2118/166526-PA.

Shi L, Gao SS, Xiong W. 2012. Physical simulation of the mechanism for operation of water-encroached (flooded) underground gas storage facilities. *Chemistry and Technology of Fuels and Oils*, **47**(6): 426-433. doi:10.1007/s10553-012-0319-2.

Shi L, Wang JM, Liao GZ, et al. 2013. Mechanism of gas-water flow at pore-level in aquifer gas storage. *Journal of Central South University*, **20**(12): 3620-3626. doi:10.1007/s11771-013-1888-x.

Sohrabi M, Tehrani D, Danesh A, et al. 2004. Visualization of oil recovery by water-alternating-gas injection using high-pressure micromodels. *SPE Journal*, **9**(3): 290-301. doi:10.2118/89000-PA.

Song YJ, Liu H, Min Z, et al. 2025. Mechanism of fault slippage in the underground gas storage and preliminary application in the Shuang 6 UGS in China. *Geoenergy Science and Engineering*, **251**: 213881. doi:10.1016/j.geoen.2025.213881.

Tang Y, Tang Z, Qin J, et al. 2025. Research on seepage and phase change characteristics during multi-cycle injection-production in oil reservoir-based underground gas storage. *Energies*, **18**(10): 2550. doi:10.3390/en18102550.

Tekseth K, Breiby D. 2024. 4D imaging of two-phase flow in porous media using laboratory-based micro-computed tomography. *Water Resources Research*, **60**(4): e2023WR036514. doi:10.1029/2023WR036514.

van Genuchten MTh. 1980. A closed-form equation for predicting the hydraulic conductivity of unsaturated soils. *Soil Science Society of America Journal*, **44**(5): 892-898. doi:10.2136/sssaj1980.03615995004400050002x.

Wang J, Feng X, Wanyan QQ, et al. 2022. Hysteresis effect of three-phase fluids in the high-intensity injection-production process of sandstone underground gas storages. *Energy*, **242**: 123058. doi:10.1016/j.energy.2021.123058.

Wang KJ, Mao HJ, Dai XJ. 2026. Experimental study on gas-water relative permeability behavior during multi-cycle injection-production in gas reservoir storage. *GeoStorage*, **2**(2): 172-179. doi:10.46690/gs.2026.02.05.

Wang YD, Blunt MJ, Armstrong RT, et al. 2021. Deep learning in pore scale imaging and modeling. *Earth-Science Reviews*, **215**: 103555. doi:10.1016/j.earscirev.2021.103555.

Wei H, Zhong Z, Cheng J, et al. 2026. The underground gas storage capacity evaluation-A case study from depleted oil reservoirs to underground gas storage. *Fuel*, **406**: 137079. doi:10.1016/j.fuel.2025.137079.

Xie C, Raeini AQ, Wang Y, et al. 2017. An improved pore-network model including viscous coupling effects using direct simulation by the lattice Boltzmann method. *Advances in Water Resources*, **100**: 26-34. doi:10.1016/j.advwatres.2016.11.017.

Yang Y, Cai S, Yao J, et al. 2021. Pore-scale simulation of remaining oil distribution in 3D porous media affected by wettability and capillarity based on volume of fluid method. *International Journal of Multiphase Flow*, **143**: 103746. doi:10.1016/j.ijmultiphaseflow.2021.103746.

Yu C, Liu W, Shang L, et al. 2026. Technological advancements and research directions for oil reservoir type underground gas storage. *Journal of Southwest Petroleum University (Science & Technology Edition)*, **48**(4): 1-10. Article online.doi:10.11885/j.issn.1674-5086.2025.12.14.02.

Zhang G, Yang S, Mo C, et al. 2022. Experimental research on capacity expansion simulation of multi-cycle injection-production in reconstruction of oil reservoir to underground gas storage. *Journal of Energy Storage*, **54**: 105222. doi:10.1016/j.est.2022.105222.

Zhang J, Tan Y, Zhang T, et al. 2020. Natural gas market and underground gas storage development in China. *Journal of Energy Storage*, **29**: 101338. doi:10.1016/j.est.2020.101338.

Zhang Q, Zheng DW, Wang J, et al. 2026c. Storage-space development and gas-liquid reorganization during cyclic injection-withdrawal in underground gas storage converted from oil reservoirs. *Geoenergy Science and Engineering*, **266**: 214673. doi:10.1016/j.geoen.2026.214673.

Zhang Q, Zheng DW, Wang J, et al. 2026a. Experimental insights into storage capacity enhancement and seepage mechanisms during multicycle injection-production in oil-reservoir-converted underground gas storage. *ACS Omega*, **11**(7): 11939-11949. doi:10.1021/acsomega.5c10025.

Zhang Q, Zheng DW, Wang J, et al.2026b. Microfluidic investigation of high-pressure high-temperature pore-scale hydrocarbon gas-water-oil three-phase flow in reservoir-type underground gas storage. *Transport in Porous Media*, **153**: Article 56. doi:10.1007/s11242-026-02303-7.

Zheng DW, Shi L, Zhang Q. 2026. Fluid mobilization mechanisms in water-invaded gas-reservoir underground gas storage under cyclic injection-withdrawal. *Energy & Fuels*, **40**(14): 7263-7279. doi:10.1021/acs.energyfuels.5c06784.

Zheng DW, Wanyan QQ, Zhao K. 2025. Development status and prospect of underground natural gas storage in China. *International Petroleum Economics*, **33**(7): 37-45. doi:10.3969/j.issn.1004-7298.2025.07.005.